ELASTIC FULL WAVEFORM TOMOGRAPHY OF SYNTHETIC MULTICOMPONENT REFLECTION SEISMIC DATA

D. Köhn, A. Kurzmann, A. Przebindowska, D. De Nil, N. Nguyen and T. Bohlen

email: *daniel.koehn@geophysik.tu-freiberg.de*

keywords: *reflection seismic imaging, waveform inversion, full wavefield*

ABSTRACT

With the increasing performance of parallel supercomputers full waveform tomography (FWT) approaches can reduce the misfit between recorded and modelled data, to deduce a very detailed physical model of the underground. In recent years acoustic waveform tomography became a very popular tool to image the underground structures. However, acoustic waveform inversion has the disadvantage, that only P waves can be inverted. It can not invert for S-waves or surface waves. Here we will present the first inversion results of our elastic parallel time domain joint FWT code for two synthetic model examples and discuss problems which occurred during the code development like preconditioning and the choice of model parameters. Even though the problem is highly nonlinear and ill conditioned the elastic FWT is able to resolve very detailed images of all three elastic model parameters.

INTRODUCTION

Full waveform tomography (FWT) is a state of the art imaging concept, which requires a massive amount of computer resources. Therefore the first applications of FWT for moderate 2D problems were undertaken in the late 1990s (Pratt (1999), Pratt and Shipp (1999)) for the acoustic case. The application of elastic FWT is even more complicated, because 3 coupled elastic parameters have to be optimized at the same time. In this paper we give a short overview of the first results we achieved with the elastic time domain FWT code DENISE (subwavelength DEtail resolving NonlInear SEismic inversion) which was developed by our working group at the TU Bergakademie Freiberg. As the name already states the FWT can only image structures at or below the seismic wavelength. The long wavelength part of the model has to be estimated by other methods like first arrival tomography. In the first section we give a short theoretical overview. Afterwards the performance of the code will be shown using two synthetic geological examples. A very simple 3 layer case and the more complex Marmousi model. We will discuss preconditioning and the influence of model parameter choice on the inversion result.

THEORETICAL BACKGROUND

The aim of full waveform tomography is to minimize the data residuals $\delta\mathbf{u} = \mathbf{d^{mod}} - \mathbf{d^{obs}}$ between the modelled data $\mathbf{d^{mod}}$ and the field data $\mathbf{d^{obs}}$. The misfit can be measured by the objective function:

$$E = \frac{1}{2}\delta\mathbf{u}^{\mathbf{T}}\delta\mathbf{u}. \tag{1}$$

The objective function can be minimized by updating the model parameters $\mathbf{m}_n$ at iteration step n using a steepest-descent gradient method:

$$\mathbf{m}_{n+1} = \mathbf{m}_n - \mu_n P\delta\mathbf{m}, \tag{2}$$

where $\delta\mathbf{m}$ denotes the steepest-descent direction of the objective function and μ_n the step length. To increase the convergence speed of the FWT code the application of a preconditioning operator P is recommended.

How to estimate $\delta\mathbf{m}$

To derive the steepest-descent direction a mapping from the data to the model space has to be found. A small change in the model space $\delta\mathbf{m}$, f.e. one model parameter at one point in space will result in a small perturbation of the data space $\delta\mathbf{d}$, f.e. one wiggle in the seismic section. If the Frechét derivative $\frac{\partial\mathbf{d}(D)}{\partial\mathbf{m}(M)}$ is known, all the perturbations in the model space can be integrated to calculate the total change in the data space:

$$\delta\mathbf{d}(D) = \int_M dM \frac{\partial\mathbf{d}(D)}{\partial\mathbf{m}(M)}\delta\mathbf{m}(M). \tag{3}$$

where M and D indicate the model and data space. If a formulation like (3) can be found, one can identify the Frechét kernel $\frac{\partial\mathbf{d}}{\partial\mathbf{m}}$ and then compute the adjoint operation - the mapping of perturbations from the data to the model space as:

$$\delta\mathbf{m}'(M) = \int_D dD \left[\frac{\partial\mathbf{d}(D)}{\partial\mathbf{m}(M)}\right]^* \delta\mathbf{d}(D). \tag{4}$$

For the elastic problem it can be shown, that the Frechét kernels are self-adjoint $\left[\frac{\partial\mathbf{d}(D)}{\partial\mathbf{m}(M)}\right]^* = \left[\frac{\partial\mathbf{d}(D)}{\partial\mathbf{m}(M)}\right]$ (Tarantola (1988)). The seismic equivalent to (3) is of the form

$$\delta u_i(\mathbf{x_s}, \mathbf{x_r}, t) = \int_V dV(\mathbf{x}) \frac{\partial u_i(\mathbf{x_s}, \mathbf{x_r}, t)}{\partial\mathbf{m}(\mathbf{x})}\delta\mathbf{m}(\mathbf{x}), \tag{5}$$

where $u_i(\mathbf{x_s}, \mathbf{x_r}, t)$ represents the seismogram located at receiver location $\mathbf{x_r}$ which records the ith component of displacement of an elastic wavefield due to a shot at $\mathbf{x_s}$.

A similar expression as (5) can be derived from the equation of motion for an isotropic elastic medium:

$$\begin{aligned} \rho\frac{\partial^2 u_i}{\partial t^2} - \frac{\partial}{\partial x_j}\sigma_{ij} &= f_i, \\ \sigma_{ij} - \lambda\epsilon_{ii}\delta_{ij} - 2\mu\epsilon_{ij} &= T_{ij}, \\ \epsilon_{ij} &= \frac{1}{2}\left(\frac{\partial u_i}{\partial x_j} + \frac{\partial u_j}{\partial x_i}\right) \\ &\quad + \text{boundary conditions}, \end{aligned} \tag{6}$$

where λ and μ denote the Lamé parameters, ρ the density, σ_{ij} the stress tensor, ϵ_{ij} the strain tensor, δ_{ij} the Kronecker Delta, f_i the volume forces and T_{ij} the surface forces. In the next step every parameter and variable in the elastic wave equation is perturbated by a first order perturbation:

$$\begin{aligned} u_i &\to u_i + \delta u_i, \\ \rho &\to \rho + \delta\rho, \\ \sigma_{ij} &\to \sigma_{ij} + \delta\sigma_{ij}, \\ \lambda &\to \lambda + \delta\lambda, \\ \mu &\to \mu + \delta\mu, \\ \epsilon_{ij} &\to \epsilon_{ij} + \delta\epsilon_{ij}. \end{aligned} \tag{7}$$

These substitutions yield a new elastic wave equation describing the displacement perturbation δu_i as a function of new source terms Δf_i and ΔT_{ij}

$$\begin{aligned} \rho\frac{\partial^2 \delta u_i}{\partial t^2} - \frac{\partial}{\partial x_j}\sigma_{ij} &= \Delta f_i, \\ \delta\sigma_{ij} - \lambda\delta\epsilon_{ii}\delta_{ij} - 2\mu\delta\epsilon_{ij} &= \Delta T_{ij}, \\ \delta\epsilon_{ij} &= \frac{1}{2}\left(\frac{\partial\delta u_i}{\partial x_j} + \frac{\partial\delta u_j}{\partial x_i}\right) \\ &\quad + \text{perturbated boundary conditions}, \end{aligned} \tag{8}$$

where the new source terms are

$$\Delta f_i = -\delta\rho \frac{\partial^2 u_i}{\partial t^2} + O(\delta\rho)^2 \tag{9}$$

and

$$\Delta T_{ij} = \delta\lambda\epsilon_{ii}\delta_{ij} + 2\delta\mu\epsilon_{ij} + O(\delta\lambda, \delta\mu)^2. \tag{10}$$

Two points are important to notice here. Equation (8) states that every change of a material parameter will act as a source ((9) and (10)), but the perturbated wavefield is propagating in the unperturbated medium. The new wave equation given in (8) has the same form as the elastic wave equation, and hence its solution can be obtained in terms of Green's functions G_{ij} of the elastic wave equation

$$\begin{aligned} \delta u_i(\mathbf{x_r}, t) = &\int_V dV(\mathbf{x}) G_{ij}(\mathbf{x_r}, t, x, 0) * \Delta f_j(\mathbf{x}, t) \\ &+ \int_S dS(\mathbf{x}) G_{ij}(\mathbf{x_r}, t, x, 0) * \Delta T_{ij}(\mathbf{x}, t). \end{aligned} \tag{11}$$

Substituting the force and traction terms given in equations (9) and (10) into equation (11), neglecting the O^2 terms (i.e., assume small perturbations in order to obtain the Frechét derivatives) gives

$$\begin{aligned} \delta u_i = &- \int_V dV \frac{\partial G_{ij}}{\partial t} * \frac{\partial u_j}{\partial t}\delta\rho - \int_V dV \frac{\partial G_{ij}}{\partial x_j} * \frac{\partial u_m}{\partial x_m}\delta\lambda \\ &- \int_V dV \frac{\partial G_{ij}}{\partial x_k} * \left(\frac{\partial u_j}{\partial x_k} + \frac{\partial u_k}{\partial x_j}\right)\delta\mu. \end{aligned} \tag{12}$$

This equation has the form as the desired expression for the forward problem (5) and so it defines the Frechét kernel $\frac{\partial u_i(\mathbf{x_s}, \mathbf{x_r}, t)}{\partial \mathbf{m}(\mathbf{x})}$, from which one may obtain the adjoint expression:

$$\delta \mathbf{m}'(\mathbf{x}) = \sum_S \int dt \sum_R \frac{\partial u_i(\mathbf{x_s}, \mathbf{x_r}, t)}{\partial \mathbf{m}(\mathbf{x})} \delta u_i(\mathbf{x_s}, \mathbf{x_r}, t), \tag{13}$$

i.e., the integral over the data space of the data residuals multiplied by the Frechét kernel. Use of (12) to solve the forward problem is known as the Born approximation. In waveform tomography the Born approximation is not used to solve the forward problem. Instead the full elastic wave equation is solved. Integrating the Frechét kernel defined by (12) over the data space produces the adjoint operation

$$\delta \mathbf{m}' = \left[\delta\lambda', \delta\mu', \delta\rho'\right]^T,$$

where

$$\begin{aligned} \delta\lambda' &= - \int dt \sum_R \frac{\partial G_{ij}}{\partial x_j} * \frac{\partial u_m}{\partial x_m}\delta u_i, \\ \delta\mu' &= - \int dt \sum_R \frac{\partial G_{ij}}{\partial x_k} * \left(\frac{\partial u_j}{\partial x_k} + \frac{\partial u_k}{\partial x_j}\right)\delta u_i, \\ &= - \int dt \sum_R \frac{1}{\sqrt{2}}\left(\frac{\partial G_{ij}}{\partial x_k} + \frac{\partial G_{ik}}{\partial x_j}\right) * \frac{1}{\sqrt{2}}\left(\frac{\partial u_j}{\partial x_k} + \frac{\partial u_k}{\partial x_j}\right)\delta u_i, \\ \delta\rho' &= - \int dt \sum_R \frac{\partial G_{ij}}{\partial t} * \frac{\partial u_j}{\partial t}\delta u_i. \end{aligned} \tag{14}$$

According to Mora (1987) these expressions can be simplified to:

$$\begin{aligned}
\delta\lambda' &= -\sum_S \int dt \left(\frac{\partial u_x}{\partial x} + \frac{\partial u_y}{\partial y}\right)\left(\frac{\partial \Psi_x}{\partial x} + \frac{\partial \Psi_y}{\partial y}\right), \\
\delta\mu' &= -2\sum_S \int dt \left(\frac{\partial u_x}{\partial y} + \frac{\partial u_y}{\partial x}\right)\left(\frac{\partial \Psi_x}{\partial y} + \frac{\partial \Psi_y}{\partial x}\right) + \left(\frac{\partial u_x}{\partial x}\frac{\partial \Psi_x}{\partial x} - \frac{\partial u_y}{\partial y}\frac{\partial \Psi_y}{\partial y}\right), \\
\delta\rho' &= -\sum_S \int dt \left(\frac{\partial u_x}{\partial t}\frac{\partial \Psi_x}{\partial t} + \frac{\partial u_y}{\partial t}\frac{\partial \Psi_y}{\partial t}\right),
\end{aligned} \tag{15}$$

where the new wavefield

$$\Psi_j(\mathbf{x}, t) = -\sum_R G_{ij}(\mathbf{x}, -t; \mathbf{x_r}, 0) * \delta u_i(\mathbf{x_r}, t) \tag{16}$$

has been introduced. This wavefield is generated by propagating the residual data δu_i from the receiver positions backwards in time.

In summary one iteration step of the FWT algorithm consists of the following steps:

1. For each shot solve the forward problem (6) for the actual model $\mathbf{m}_n$ to generate a synthetic dataset $\mathbf{d^{mod}}$ and the wavefield $\mathbf{u}(\mathbf{x}, t)$.
2. Calculate the residual seismograms $\delta\mathbf{u} = \mathbf{d^{mod}} - \mathbf{d^{obs}}$.
3. Generate the wavefield $\mathbf{\Psi}(\mathbf{x}, t)$ by backpropagating the residuals from the receiver positions.
4. Calculate the optimal perturbations $\delta\mathbf{m}$ of each material parameter according to (15).
5. Apply an appropriate preconditioning operator P.
6. Estimate the step length μ_n by a line search.
7. Update the material parameters using the gradient method $\mathbf{m}_{n+1} = \mathbf{m}_n - \mu_n P \delta\mathbf{m}$.

In our FWT code the forward problem and backpropagation of the residual wavefield are solved using a parallel time domain finite difference code (Bohlen (2002)). In the following sections two synthetic FWT test problems will be presented to demonstrate the performance of the code.

A SIMPLE GEOLOGICAL TEST PROBLEM

For first parameter tests a simple geological model was used, which consists of a free surface, a water column, two layers with undulating interfaces and a half space (Fig. 1, bottom). The S-wave velocity V_s and density ρ are calculated from the P-wave distribution V_p using the following relationships:

$$\begin{aligned}
V_s &= V_p/\sqrt{3}, \\
\rho &= 0.31 * 1000.0 * V_p^{1/4}.
\end{aligned} \tag{17}$$

Using an 8th order spatial FD operator the model could be discretized with 640×600 gridpoints in x- and y-direction with a spatial gridpoint distance of 2.5 m. The time was discretized using DT = 0.54 ms, thus for a recording time of T = 1.5 s 2777 time steps are needed. The acquisition geometry consists of an Ocean Bottom Cable (OBC) on the sea floor with 93 two component receivers. 20 airgun shots were recorded with a shot distance of 69 m. The source signature was a 30 Hz Ricker wavelet. The calculation time using 64 CPUs on an ALTIX 4700 for one iteration step is roughly 3.5 minutes.

As mentioned above even very simple preconditioning operators can increase the convergence speed of the FWT code significantly. To correct the amplitude loss at greater depth due to reflections and spherical divergence in a reflection geometry a simple scaling of the gradient with depth $\mathrm{P} = \mathrm{depth^n}$, where n is an integer number, can be applied. For the synthetic tests n=3 works very well.

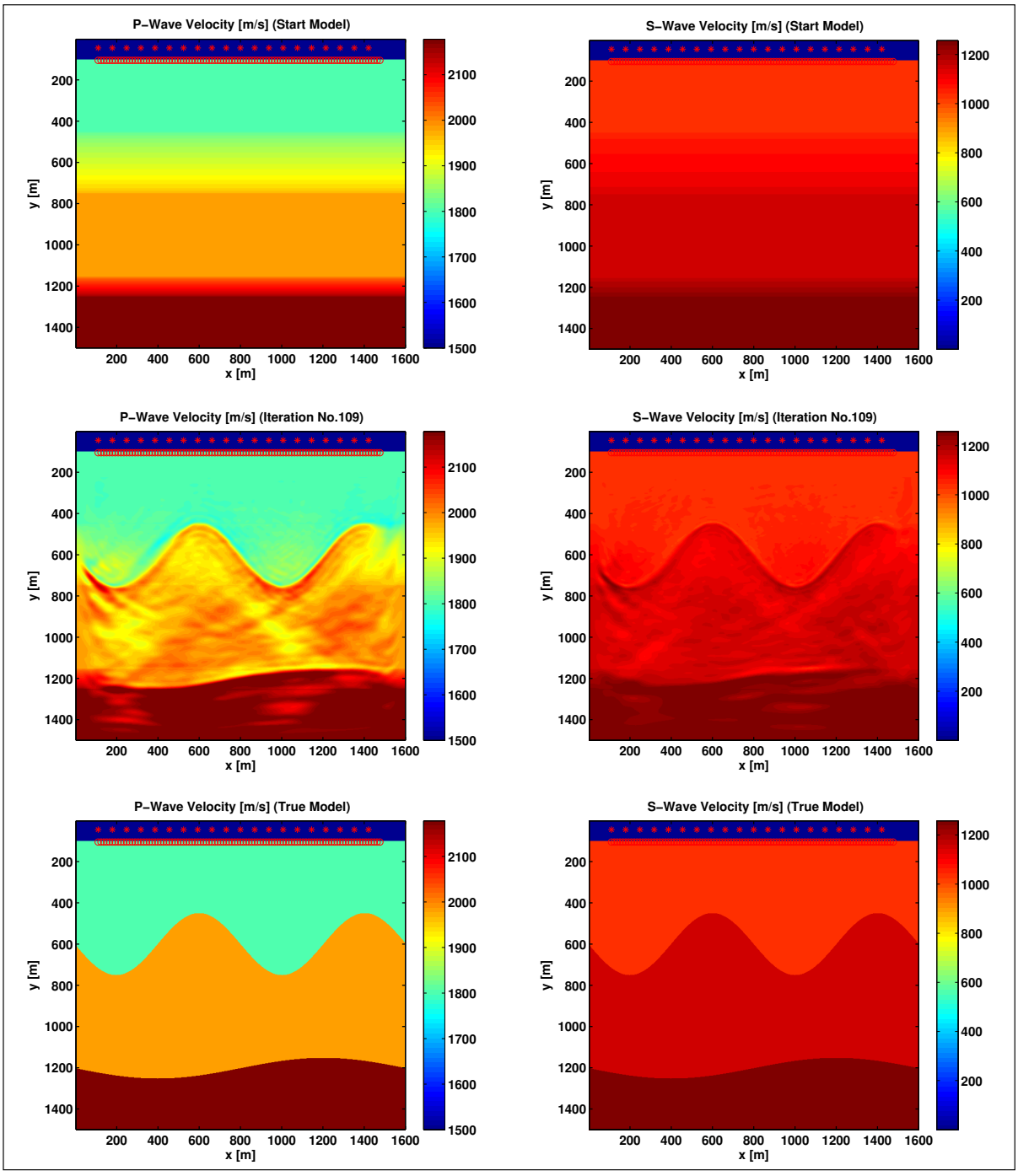

Figure 1: Simple Geological Test Problem: P-wave velocity (left column), S-wave velocity (right column). 1D staring model (top), Inversion result after 110 iteration steps (center), true model (bottom).

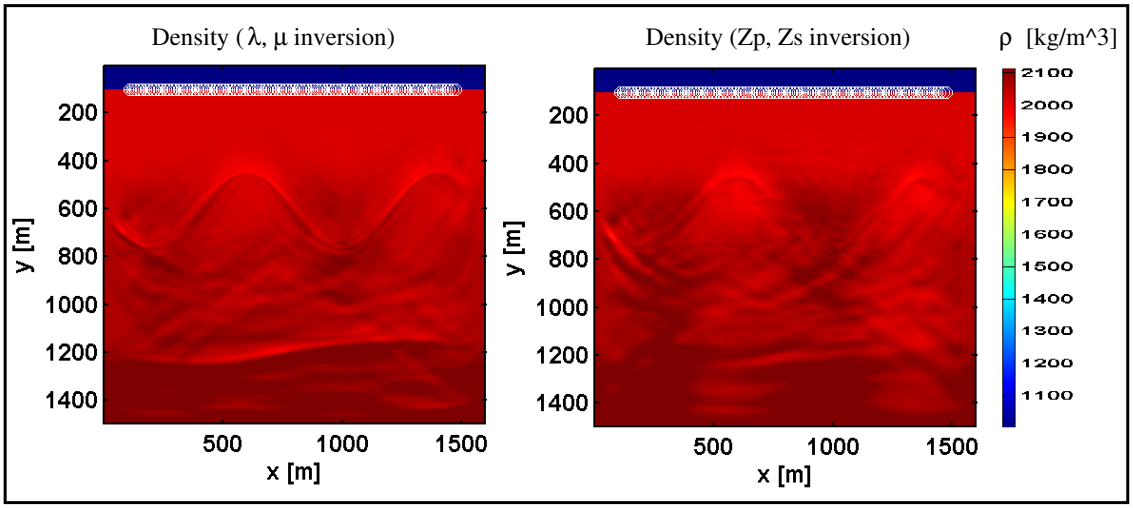

Figure 2: Density inversion results for the simple geological problem using the Lam*é* parameters (left) and the impedances (right) as model parameters in the FWT.

For the isotropic elastic wave equation, the most obvious choice of model parameters $\mathbf{m}$ are the Lamé parameters λ, μ and the density ρ. The inversion results for this parameter set are shown in Fig. 1 (center). For better comparison the Lam*é* parameters are converted to seismic velocities. The interface locations and velocities could be reconstructed very well from the 1D starting model (Fig.1 (top)). There are other choices of model parameters which are more physically meaningful and better resolved (Tarantola (1986)), but we think might not be optimal for a joint multiparameter inversion. To demonstrate that problem the gradients are rewritten in terms of P-wave impedance Zp and S-wave impedance Zs (Mora (1987)):

$$\begin{aligned} \delta Z_p &= 2V_p\delta\lambda', \\ \delta Z_s &= -4V_s\delta\lambda' + 2V_s\delta\mu', \\ \delta\rho &= (V_p^2 - 2V_s^2)\delta\lambda' + V_s^2\delta\mu' + \delta\rho'. \end{aligned} \tag{18}$$

The comparison of the density update function in (18) and (15) shows that for the impedances the density update depends on the gradients $\delta\lambda'$, $\delta\mu'$ and the actual seismic velocities, while the density update for the Lam*é* parameters is independent of all the other parameters. In Fig. 2 the inversion results for the density are shown. While the Lam*é* parameters (left) can easily resolve the interfaces, the impedance result (right) is not capable to resolve the correct density distribution and is dominated by artefacts.

A COMPLEX GEOLOGICAL TEST PROBLEM - THE ELASTIC MARMOUSI MODEL

A widely used test problem for seismic imaging techniques is the elastic Marmousi II model (Martin et al. (2006)). The model consists of horizontal layers near the boundaries, while steep thrust faults are disturbing the layers in the center of the model. These thrust faults are not easy to resolve by conventional first arrival tomography, so it is an ideal test model for the FWT. Due to computational restrictions the original Marmousi II model could not been used, because the very low S-wave velocities in the sediments would require a too small spatial sampling of the model. Therefore new S-wave velocities and densities were calculated from the P-wave velocities using the scaling relations (17).

Using an 8th order spatial FD operator the model could be discretized with 1000×580 gridpoints in x- and y-direction with a spatial gridpoint distance of 5.0 m. The time was discretized using DT = 0.54 ms, thus for a recording time of T = 2.5 s 4630 time steps are needed. The acquisition geometry consists of an OBC on the sea floor with 301 two component receivers. 41 airgun shots were recorded with a shot distance of 112 m. The source signature was a 20 Hz Ricker wavelet. The calculation time using 50 CPUs on an ALTIX 4700 for one iteration step is roughly 30 minutes.

Due to the results of the last section, we choose the Lam$\acute{e}$ parameters as model parameters for the inversion. The starting model, inversion result after 100 iterations and the true model are shown as P-wave velocity, S-wave velocity and density in Fig. 3 - 5. The starting model is a Gauss filtered version of the true model with a correlation length $\lambda_c = 100.0\ m$. To achieve a smooth transition from the long wavelength starting model to the inversion result with short wavelength structures the application of a frequency filter with variable bandwidth on the data residuals $\delta\mathbf{u}$ is vital, to avoid the convergence into a local minimum. In this case a low pass filter with the following characteristics was used during the first iteration: f1=0.0 Hz, f2=0.0 Hz, f3=5.0 Hz, f4=10.0 Hz, amps=1.,1.,1.,0.. Between f3 and f4 a Gaussian taper function is applied. At all subsequent iteration steps the bandwidth was increased by 0.46 Hz/iteration step, so until the 100th iteration the full spectral content was inverted.

Even though the coverage was not very high the inversion results are showing a lot of small details and fine layers which are absent in the starting model. The thrust faults are also imaged very well. Even the density, a parameter which can be hardly estimated from seismic data, is resolved well. In Fig. 6 the seismic sections of shot 10 are plotted for the starting model (top), the inversion result (center) and the true model (bottom). Notice the good fit of the first arrivals for the starting model, but the lack of small details beyond the first arrivals. The inversion result fits the phases and amplitudes of the later small scale arrivals very well.

CONCLUSIONS AND OUTLOOK

In this paper we have shown the potential of elastic FWT for imaging structures which are on the same scale or smaller than the seismic wavelength. The success of FWT depends not only on the preconditioning of the gradients, but also on the choice of model parameters. The chosen preconditioning was a very simple scaling of the gradients. More sophisticated operators might improve the inversion result and increase the convergence speed of the code. For a successful joint inversion of all three elastic parameters it is essential to choose the Lam$\acute{e}$ parameters as model parameters, because other parameter sets can not be inverted independently. Another problem, if not the biggest, is the estimation of the starting model. Currently we are testing different methods for searching the long wavelength parameter space to estimate plausible starting models for the FWT. If all this research is done we will start with the elastic inversion of ultrasonic and real streamer/OBC data.

REFERENCES

Bohlen, T. (2002). Parallel 3-D viscoelastic finite-difference seismic modelling. *Computers & Geosciences*, 28(8):887–899.

Martin, G., Wiley, R., and Marfurt, K. (2006). Marmousi2 - An elastic upgrade for Marmousi. *The Leading Edge*, 25:156–166.

Mora, P. (1987). Nonlinear two-dimensional elastic inversion of multioffset seismic data. *Geophysics*, 52:1211 – 1228.

Pratt, R. (1999). Seismic waveform inversion in the frequency domain, Part 1: Theory and verification in a physical scale model. *Geophysics*, 64:888–901.

Pratt, R. and Shipp, R. (1999). Seismic waveform inversion in the frequency domain, Part 2: Fault delineation in sediments using crosshole data. *Geophysics*, 64:902–914.

Tarantola, A. (1986). A strategy for nonlinear elastic inversion of seismic reflection data. *Geophysics*, 51:1893–1903.

Tarantola, A. (1988). Theoretical background for the inversion of seismic waveforms, including elasticity and attenuation. *PAGEOPH*, 128:365–399.

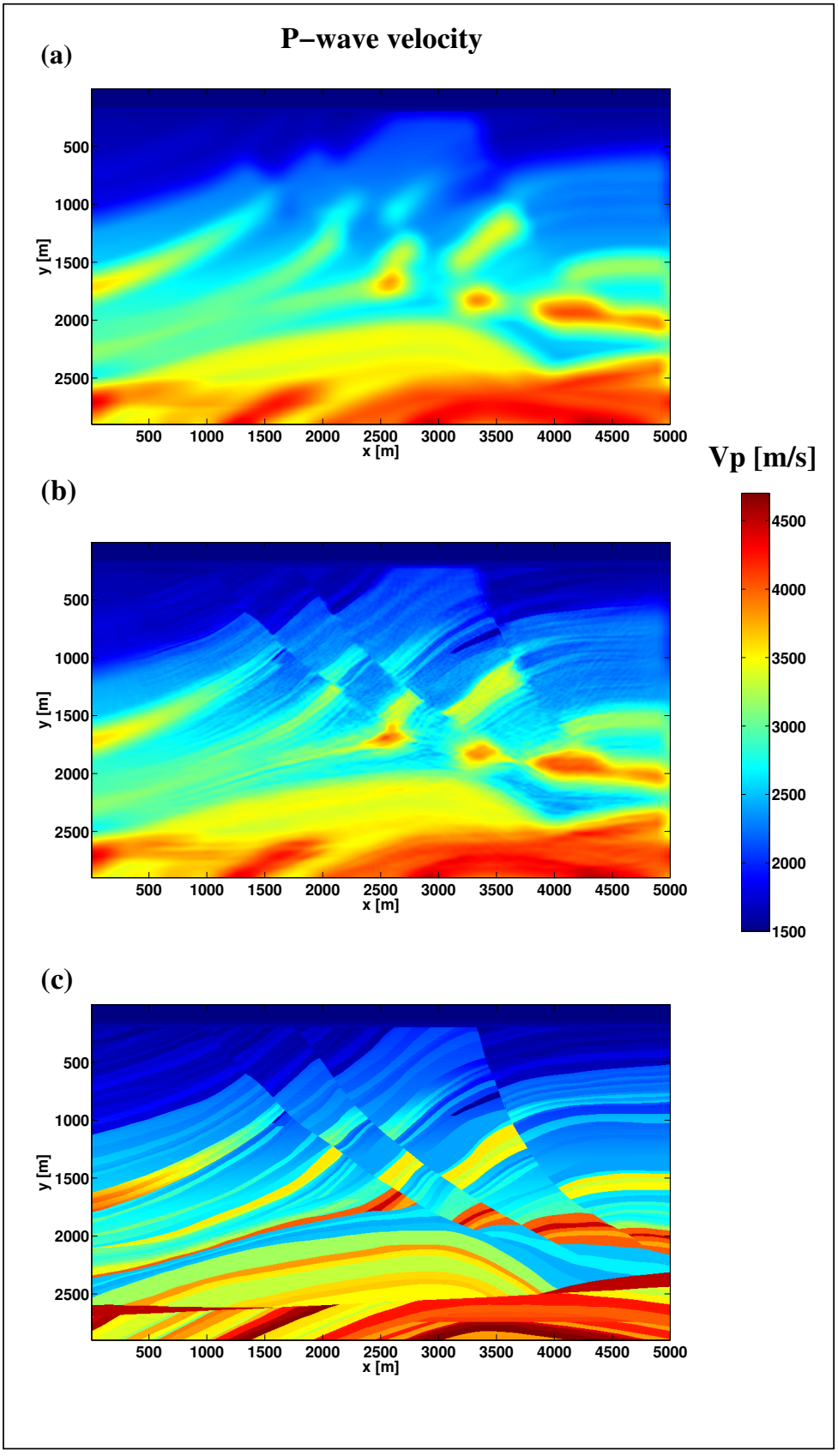

Figure 3: P-wave velocity Marmousi model: (a) starting model, (b) inversion result, (c) true model.

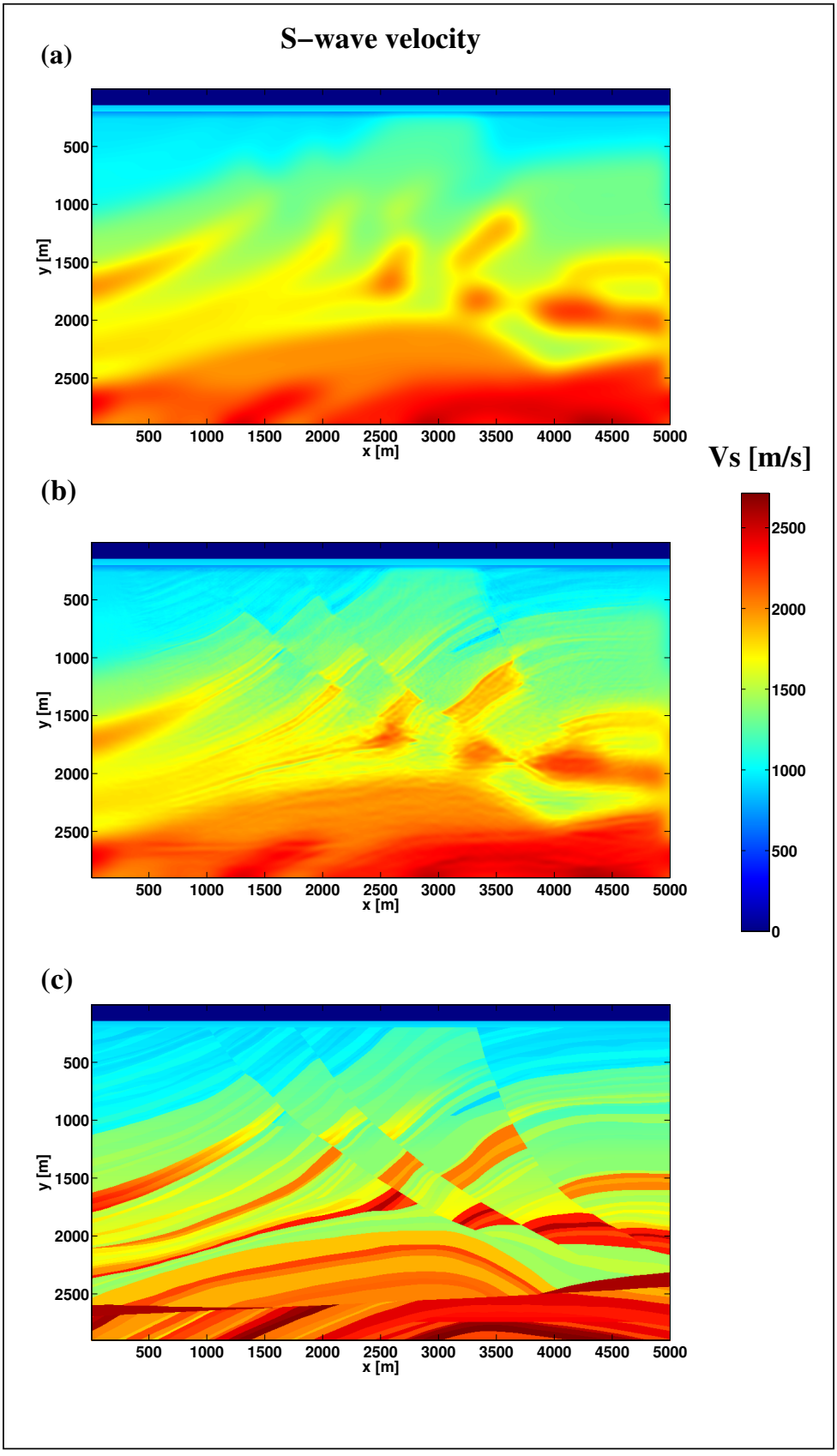

Figure 4: S-wave velocity Marmousi model: (a) starting model, (b) inversion result, (c) true model.

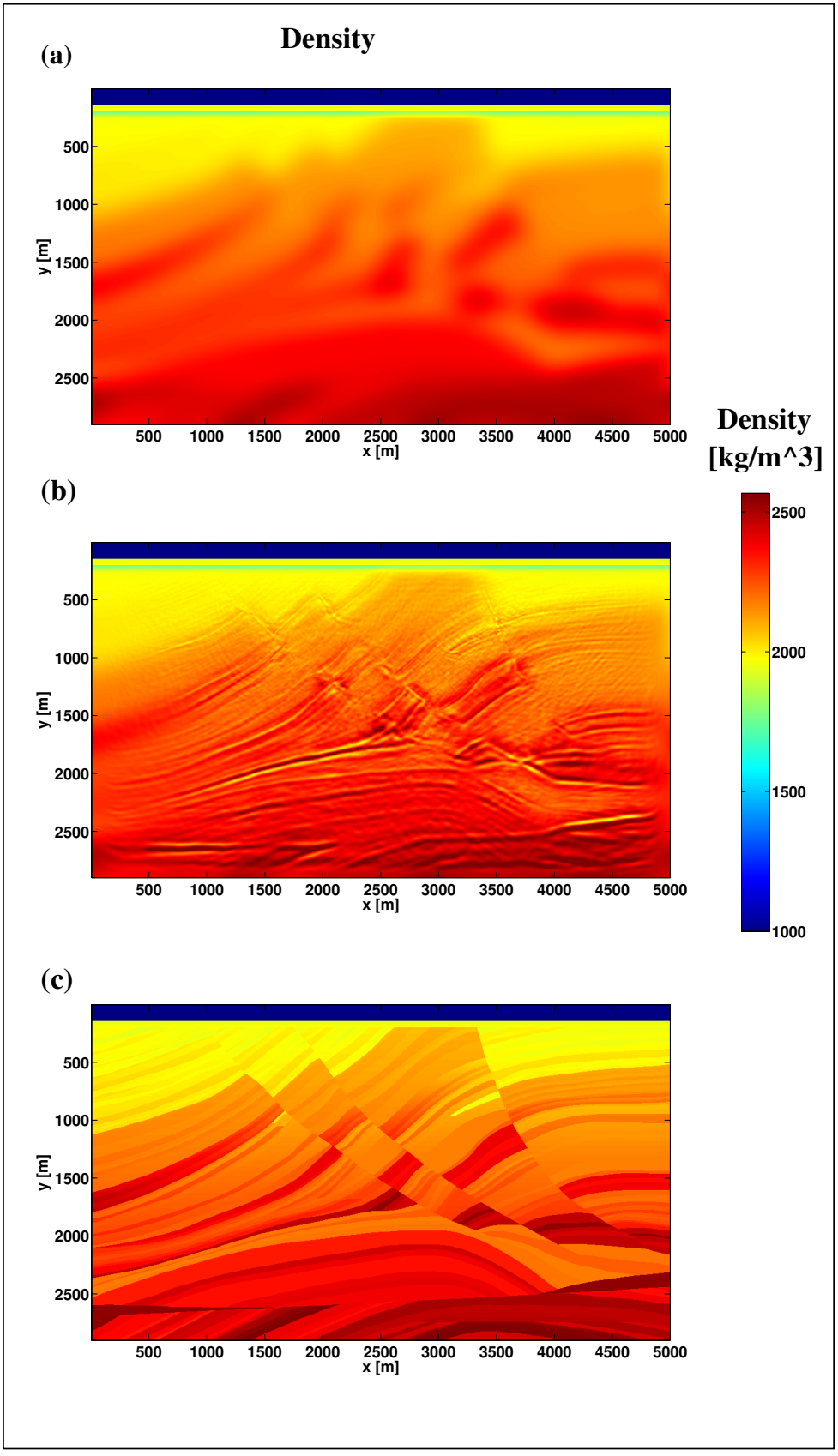

Figure 5: Density Marmousi model: (a) starting model, (b) inversion result, (c) true model.

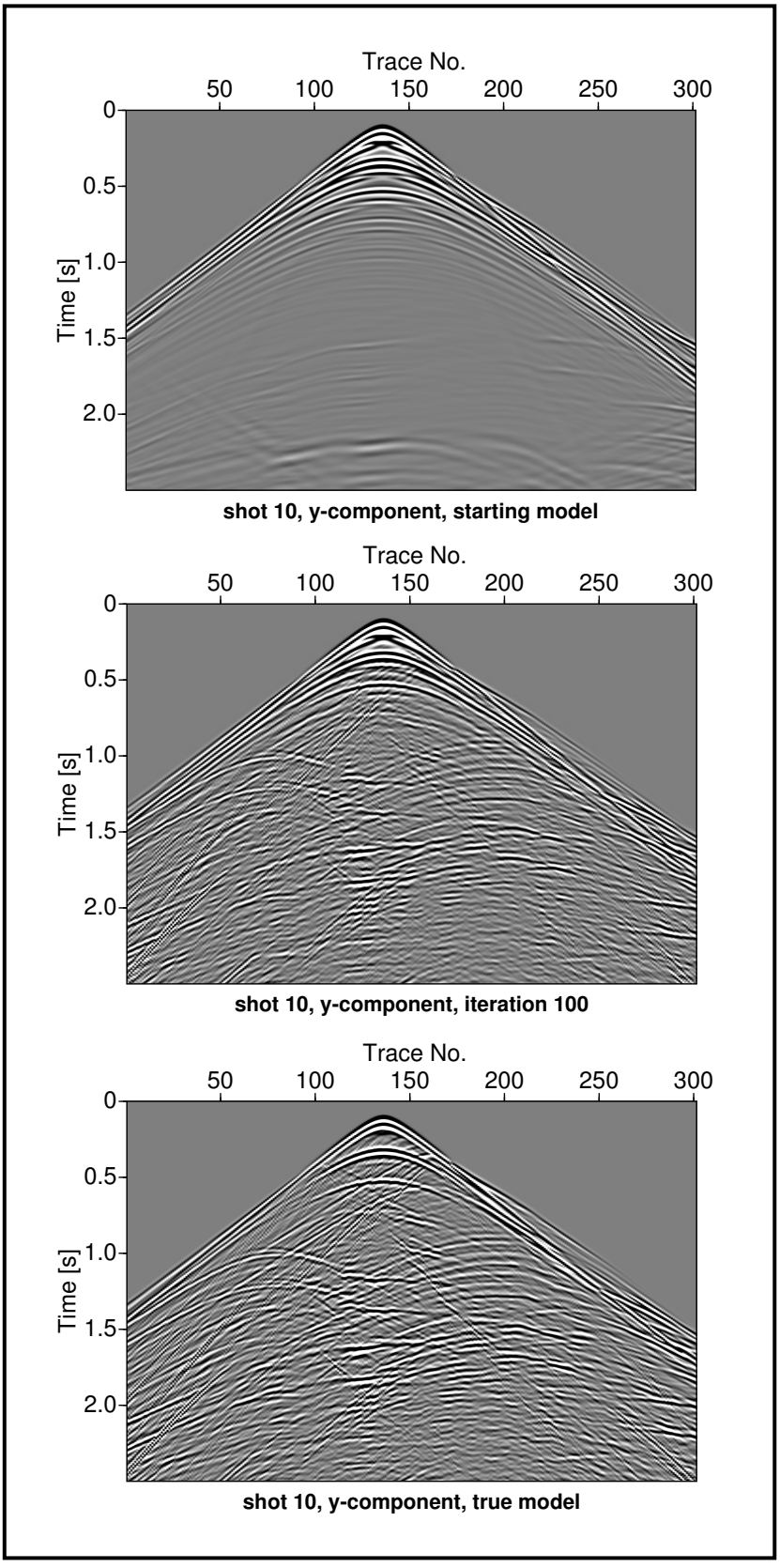

Figure 6: Seismic sections for the Marmousi model (shot 10, y-component): The starting model (top), the inversion result (center) and the true model (bottom).